Positron annihilation response and broadband dielectric spectroscopy: Salol

J. Bartoš[1,a], M. Iskrová[2], M. Köhler[3], R. Wehn[3], O. Šauša[2], P. Lunkenheimer[3], J. Krištiak[2], and A. Loidl[3]

[1] Polymer Institute of SAS, Dúbravská cesta 9, SK - 845 41 Bratislava, Slovak Republic
[2] Institute of Physics of SAS, Dúbravská cesta 9, SK - 842 28 Bratislava, Slovak Republic
[3] Experimental Physics V, Center for Electronic Correlations and Magnetism, University of Augsburg, D - 86135 Augsburg, Germany

Abstract. A phenomenological analysis of the ortho-positronium (o-Ps) annihilation from positron annihilation lifetime spectroscopy (PALS) and the dynamics from broadband dielectric spectroscopy (BDS) are reported on a small molecular glass former of intermediate H-bonding and fragility: *salol*. The dielectric spectra extend over a very broad frequency range of about 2×10^{-2}–3.5×10^{11} Hz, providing information on the α-relaxation, the secondary relaxation giving rise to the excess wing, and the shallow high-frequency minimum in the micro- to milli-meter wave range. A number of empirical correlations between the o-Ps lifetime, $\tau_3(T)$, and the various spectral and relaxation features have been observed. Thus, the phenomenological evaluation of the $\tau_3(T)$ dependence of the PALS response of the amorphous sample reveals three characteristic PALS temperatures: $T_g^{\rm PALS}$, $T_{b1}^L = 1.15T_g^{\rm PALS}$ and $T_{b2}^L = 1.25T_g^{\rm PALS}$, which are discussed in relation to similar findings for some typical small molecular vdW- and H-bonded glass formers. A slighter change of the slope at T_{b1}^L appears to be related to the transition from excess wing to the primary α-process-dominated behavior, with the secondary process dominating in the deeply supercooled liquid state below T_{b1}^L. The high-temperature plateau effect in the $\tau_3(T)$ plot occurs at T_{b2}^L and agrees with the characteristic Stickel temperature, $T_B^{\rm ST}$, marking a qualitative change of the primary α process, but it does not follow the relation $T_{b2}^L < T_\alpha$ [$\tau_3(T_{b2}) < \tau_\alpha$]. Both effects at T_{b1}^L and T_{b2}^L correlate with two crossovers in the spectral shape and related non-exponentiality parameter of the structural relaxation, $\beta_{\rm KWW}$. Finally, the application of the two-order parameter (TOP) model to the structural relaxation as represented by the primary α relaxation times from BDS leads to the characteristic TOP temperature, T_m^c, close to T_{b1} from PALS. Within this model the phenomenological interpretation is offered based on changes in the probability of occurrence of solid-like and liquid-like domains to explain the dynamic as well as PALS responses. In summary, all the empirical correlations support further very close connections between the PALS response and the dielectric relaxation behavior in small molecule glass formers.

1 Introduction

Solidification of small molecular or polymeric liquids into the solid state can occur by crystallization or/and by glassification. In contrast to the first type of transition, the origin of the dynamic slowdown of the liquid during cooling as well as of the closely related liquid-to-glass transition phenomenon is a timely and still unresolved topic in the physics and chemistry of disordered materials [1–4]

Classical X-ray and neutron scattering studies show slight variations in the main diffraction peaks and seem to suggest a rather monotonous structural change over a wide temperature range on going from the rapidly relaxing normal liquid towards the very slowly relaxing glass [5–7] where the relaxation dynamics varies over 14–16 orders of magnitude [1–4]. On the other hand, detailed dynamic studies of small molecule and polymer glass formers revealed that the dynamic heterogeneity as a function of temperature in both frequency and time domains is an important aspect of disordered systems [8–15]. Usually, several distinct regions of the temperature behaviour of the relaxation time are marked by the corresponding characteristic dynamic temperatures such as the Arrhenius T_A [16–19], Stickel $T_B^{\rm ST}$ [20–22] and Schönhals $T_B^{\rm SCH}$ [23] temperatures. In addition, the non-exponentiality coefficient, $\beta_{\rm KWW}$, of the Kohlrausch-Williams-Watts (KWW) equation as a function of temperature exhibits often —but not always— the existence of two regions of distinct behavior marked by the characteristic temperature, $T_B^{\beta_{\rm KWW}}$ [24–26]. Intriguing features

[a] e-mail: Jozef.Bartos@savba.sk

of these dynamic crossovers at the characteristic dynamic temperatures, $T_B^{\rm ST}$ and T_A, are that the corresponding structural relaxation times or viscosities are material constants invariant to both temperature and pressure [27–31]. All these empirical dynamic findings appear to be indicators of subtle changes in motional regimes of the glass formers [8–11].

Evidently, the explanation of the physical origin of these dynamically distinct regions over a wide T interval and the closely related crossover temperatures can significantly contribute to our understanding of the vitrification phenomenon in various types of glass formers [8–11]. Several phenomenological approaches based on the extended free volume (EFV) model [32–35], the coupling model (CM) [36–38] and frustrated-limited domains (FLD) model [39–41] have been proposed to interpret the physical nature of these characteristic dynamic temperatures. Recently, a joint diffraction and computer modeling work indicated the presence of cluster-like heterogeneities in a few amorphous glass formers [42]. These structural findings could be plausibly explained in terms of solid- and liquid-like domains of the hetero-phase fluctuation (HPF) [43,44] or the two-order parameter (TOP) model [45–48].

Alternatively, the structural-dynamic state of glass formers can be treated in terms of a simple and physically plausible free-volume concept serving as a measure of the structural disorder or/and the mobility of the constituents of condensed material. This concept became a very useful idea in the interpretation of the thermodynamic, dynamic and transport properties [49–51]. In this context, positron annihilation lifetime spectroscopy (PALS) is a unique, highly relevant method sensitive to the evolution of different dynamic-related structures. PALS is based on detection of the annihilation behavior of the atomic ortho-positronium (o-Ps) probe, *i.e.*, a bound system of a positron and an electron which is formed and localized in local static (permanent) or dynamic (transient) regions of reduced electron density, *i.e.* vacancies or free volume holes [52–54]. The o-Ps lifetime, τ_3, due to pick-off interaction with an electron with the opposite spin in the surrounding medium is a measure of the size of these free-volume regions [55–57]. Thus, this method is an effective tool for the free-volume characterization of crystalline and amorphous condensed materials.

In crystalline substances, the o-Ps lifetime as a function of temperature, $\tau_3(T)$, exhibits two distinct regions corresponding to the defect ordered (real crystal) and disordered (normal liquid) phase with a sharp step effect close to the thermodynamic melting temperature, T_m [58–60]. On the other hand, the PALS response of amorphous glass formers is more complex. Basically, the sigmoidal or quasi-sigmoidal dependence of $\tau_3(T)$ extends over a wide temperature range and is finished by a pronounced plateau or quasi-plateau effect at higher temperatures with respect to T_g [61–65]. Phenomenological analyses of the $\tau_3(T)$ plots for a series of small molecule and polymer glass formers revealed several regions of a distinct linear behavior marked by the characteristic PALS temperatures which, according to a unified notation [65], are denoted as T_{b1}^G [65], $T_g^{\rm PALS}$, T_{b1}^L [65–69] and $T_{b2}^L = T_r = T_k$ [62–65,70,71]. The first temperature lies at $T_{b1}^G \cong (0.6\text{–}0.8)T_g^{\rm PALS}$ [65] and the two latter ones are localized at $T_{b1}^L \cong (1.2\text{–}1.4)T_g^{\rm PALS}$ [65–69] and $T_{b2}^L \cong (1.2\text{–}1.7)T_g^{\rm PALS}$ [62–65,70–75].

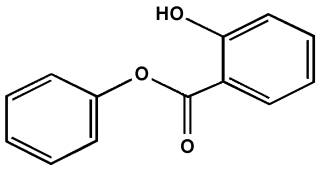

Fig. 1. Chemical structure of *salol*.

For better understanding, the PALS response should be compared with the responses of traditional techniques indicating thermodynamic and/or dynamic changes at the various characteristic temperatures. At present, certain relationships between various features of the PALS response and those in viscosity [16–18] or dielectric spectra [19–26, 76,77] suggest to some extent a dynamic character of the PALS response in the liquid state, at least. Thus, it was early revealed [70] that an onset of the (quasi-) plateau in the PALS response at T_{b2}^L lies close to the Arrhenius temperature, T_A, above which the structural, *i.e.* viscosity [16–18] or primary α-relaxation [19,77], dynamics behaves approximately in the thermally activated fashion. Recent advances in BDS [76,77] enabled to reveal further connections between the PALS response and the glassy dynamics [65,78–84]. Thus, two empirical T_{b2}^L and T_{b1}^L rules establish the specific relationships between the o-Ps lifetime, τ_3, and the primary α-relaxation time, τ_α, namely, $\tau_\alpha(T_{b2}^L) \sim 10^{-9}$ s or $\tau_\alpha(T_{b1}^L) \sim 10^{-6\pm1}$ s, respectively [65, 78]. In the former case, in addition, for many glass formers at the onset of the plateau or quasi-plateau effect in the PALS response the relation $\tau_3 \cong \tau_\alpha$ has often been found. Moreover, in some small molecule and polymer glass formers T_{b2}^L lies in the vicinity of the characteristic dynamic temperatures such as Stickel, $T_B^{\rm ST}$, or Schönhals, $T_B^{\rm SCH}$, ones, where the structural relaxation changes qualitatively its character [65,66,72–74,79–83], whereas in other cases T_{b1}^L is situated close to the $T_B^{\rm ST}$ [82]. The observation seems to suggest some role of the primary α process in the PALS response but indications about a possible influence of the slow secondary relaxations in a few small molecular glass formers were also suggested [78,82–84]. This issue is still unclear and requires further systematic combined investigations and accumulation of the data.

In the glass science community, *phenyl-2-hydroxybenzoate* or *phenyl salicylate* (*salol*) is an often studied small-molecule glass former for its relative simple chemical structure of the internally flexible molecules (fig. 1) with intermediate H-bonding and fragility $m_g = 63$ [85] or 73 [86] lying between a typical strong glass former of the rigid molecules with extensive H-bonding such as *glycerol* (GL) ($m_g = 53$) [85,86] and a typical fragile one of the rigid entities with vdW intermolecular interactions such as *propylene carbonate* (PC) ($m_g = 104$) [85,86]. *Salol* was investigated by structural [42,87–89], thermodynamic [90]

and a series of various dynamic techniques including viscosity [91–93], dielectric spectroscopy [19,20,28,94–96], light scattering [97,98] and ESR [99]. Very recently, G. Dlubek *et al.* have investigated the free-volume microstructure of *salol* by the PALS method in a simple heating regime only in combination with PVT study and discussed its relaxation dynamics from a point of view of the hole lattice model [100]. In our contribution, we present a more detailed PALS study including various heating and cooling measuring cycles together with a phenomenological analysis of the PALS response using the detailed relevant dielectric data. Such a joint approach reveals some further new connections between the o-Ps annihilation and the spectral and relaxation characteristics of dipolar relaxation. This underlines further the existence of a close relationship between the PALS characteristics and various dynamic parameters and points to the dynamic character of the PALS response.

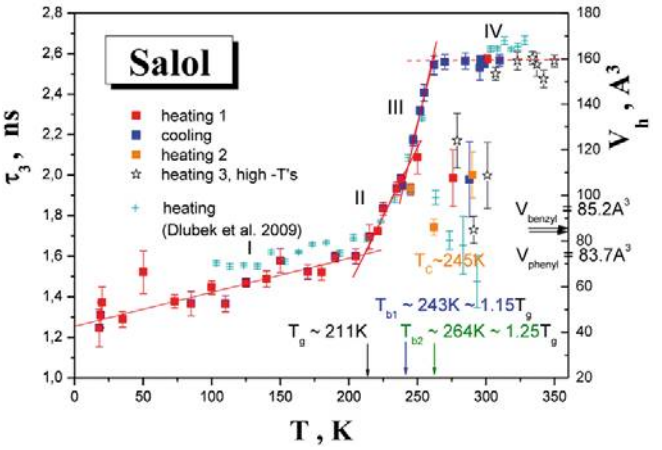

Fig. 2. o-Ps lifetime, τ_3, and mean free volume hole, V_h, as a function of temperature T for *salol*. For the details of the various measuring cycles —see the text. The o-Ps lifetime data from the recent PALS measurement in the heating regime are also included [100].

2 Experimental

Salol with a purity of 99% was obtained from Aldrich Inc. and used as received.

2.1 PALS method

The positron annihilation lifetime spectra of *salol* were obtained at the Institute of Physics of SAS, Bratislava by the conventional fast-fast coincidence method using plastic scintillators coupled to Phillips XP 2020 photomultipliers. The time resolution of prompt spectra was about 320 ps. The radioactive positron ^{22}Na source plus samples assembly was kept under vacuum in cryogenerator. During the low-temperature measurements from 15 K up to 300 K, samples in a holder were fixed at the end of a cold finger of a closed-cycle refrigerator Leybold with automatic temperature regulation. The higher temperature study above RT was performed in a chamber without vacuum. The stability of temperature was about 1 K [101]. The positron lifetime spectra were analyzed using the well-known PATFIT-88 software package [102] in terms of a short-term component from *para*-positronium *p*-Ps, τ_1, an intermediate one attributed to "free" positron, τ_2, and a long-term one, related to free volume: *ortho*-positronium *o*-Ps, τ_3. The acquisition time per each temperature point was at least 2 hours. The different heating and cooling cycles have been chosen to observe a crystallization and a glassification.

2.2 BDS method

Broadband dielectric measurements of the same *salol* sample have been performed at the University of Augsburg using a combination of different techniques enabling to cover nearly 20 decades in frequency [76,103–107]. In the low-frequency range a frequency response analyzer (Novocontrol α analyzer, 10^{-3} Hz $< \nu <$ 10 MHz) was used. For the radio-frequency and microwave range (1 MHz $< \nu <$ 2 GHz), a reflectometric technique was employed, with the sample capacitor mounted at the end of a coaxial line [105]. These measurements were performed with the HP 4291 impedance analyzer. For all the above-mentioned methods, the sample material was filled into parallel-plate capacitors. In the region 100 MHz–25 GHz coaxial transmission measurements using the HP 8510 network analyzer were carried out [103]. These measurements require filling the sample material into a specially designed coaxial line, sealed with Teflon discs. At frequencies 60 GHz $< \nu <$ 1.2 THz, a quasi-optical sub-millimeter spectrometer [106,107] was used with an experimental arrangement similar to a Mach-Zehnder interferometer (for more details, see refs. [103,106,107]). For temperature variation, closed-cycle refrigerators and N_2-gas cryostats were used.

3 Results

3.1 PALS results

Figure 2 displays the o-Ps lifetime, τ_3, as a function of temperature for *salol* as measured over an extraordinary wide temperature range from 15 K up to 350 K. Several measuring cycles are included: i) heating cycle No. 1 from 15 K up to RT after rapid cooling (2 K min) the previously melted sample from RT; ii) slow cooling cycle from RT down to 15 K followed by iii) heating cycle No. 2 from 15 K up to RT and finally, iv) heating cycle No. 3 from RT up to 350 K. Qualitative differences in the corresponding PALS responses dependent on the measuring cycle are evident. Thus, in both the heating cycles No. 1 and 2, on crossing a pronounced bend effect at around 210 K a dramatic decrease at $\sim$ 245 K followed by a rapid increase at 300 K which lies on the plateau of the total PALS response is observed. On the other hand, in a cooling cycle

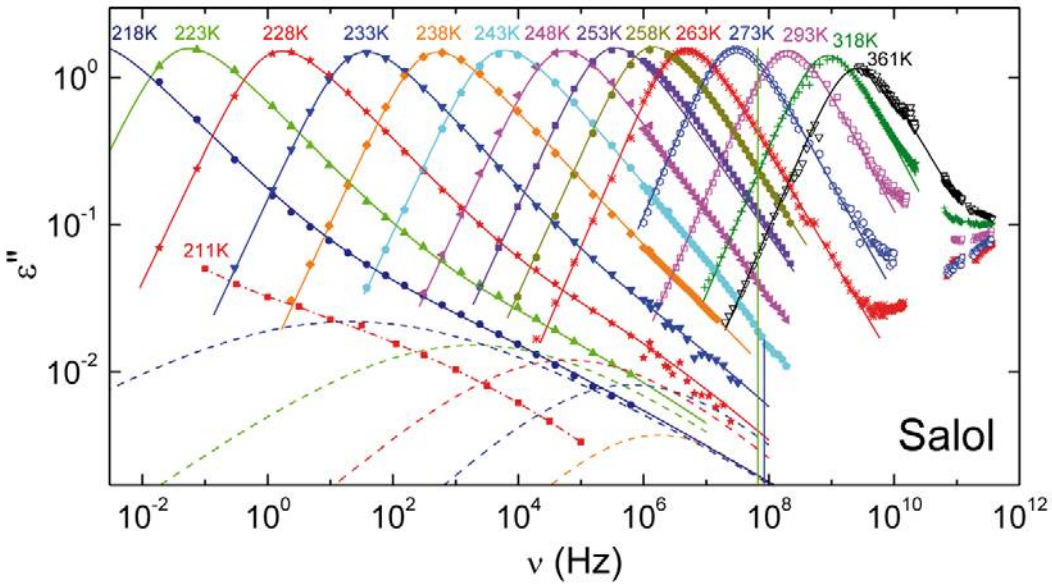

Fig. 3. (Colour on-line) Dielectric loss as a function of frequency at a series of temperatures from 211 K up to 361 K for *salol*. The solid lines are fits with a HN function for $T \geq 243$ K and with the sum of a HN and CC function for $T \leq 238$ K. The dashed lines show the CC components. The dash-dotted line through the 211 K data is a guide to the eyes. The vertical lines mark the equivalent frequencies, $\nu(T_{bi})$ corresponding to the o-Ps lifetime values at T_{b1} (blue) and T_{b2} (green).

we find an onset of the decrease at around 265 K but with no signature of any dramatic decrease in τ_3 in the temperature range around 240–250 K as for the heating cycles after rapid cooling. On further cooling, the corresponding curve follows that from the heating one down to 15 K. Subsequent heating scan on this relatively slowly cooled sample reproduces the first heating cycle obtained after relatively rapid cooling. Figure 2 contains also the Dlubek's *et al.* data from a heating scan after relative rapid cooling the melted sample from ref. [100]. Their τ_3 values are in quite reasonable agreement with our two heating cycles. Similar PALS responses have been recently observed for other small molecular crystallizing glass formers —see, *e.g.*, *diethylphtalate* [80].

3.2 BDS results

Figure 3 shows the dielectric loss, ε'', of the same *salol* material as a function of frequency for a series of temperatures from 211 K up to 361 K [108,109]. The dielectric response of *salol* over an extremely wide frequency range from about 2×10^{-2} Hz up to 3.5×10^{10} Hz exhibits a spectral evolution typical for type-A glass formers [110] with a large main peak at lower frequencies and without any smaller one at the higher ones. Instead, a so-called excess wing (EW), *i.e.*, a second power law at the high-frequency flank of the main peak is observed. The main peak is attributed to the structural relaxation, *i.e.*, the primary α process, while the EW is ascribed to a submerged slow secondary relaxation [111–114]. The latter fact becomes obvious from the slight but significant curvature of the spectrum at 211 K. This sub-T_g curve has been measured after aging for 6.5 days to ensure that the sample is in thermodynamic equilibrium as discussed in detail in ref. [112]. Finally, at the highest frequencies, $\nu > 10^{10}$ Hz, a rather shallow loss minimum shows up. The present data belong to the relatively few examples of glass-forming liquids [76,104,115–118] where a sufficiently broad frequency range has been covered to detect this minimum. It is often interpreted in terms of the so-called fast β relaxation of the mode coupling theory but also other explanations have been proposed [76]. An analysis of the minimum region of salol is out of the scope of the present work and will we provided in a subsequent paper.

Phenomenological analysis of the BDS spectra used here was based on a deconvolution procedure assuming an additive scheme. The spectral and relaxation parameters of the individual relaxation modes in *salol* are obtained by using the Havriliak-Negami (HN) [77,119] and Cole-Cole (CC) [77,120] function for the primary α process or for the secondary β process, respectively:

$$\varepsilon'' = -\operatorname{Im}\{\Delta\varepsilon_{\rm HN}/[1+(i\omega\tau_{\rm HN})^{(1-\alpha_{\rm HN})}]^{\beta_{\rm HN}} + \Delta\varepsilon_{\rm CC}/(1+i\omega\tau_{\rm CC})^{(1-\alpha_{\rm CC})}\}, \quad (1)$$

where $\Delta\varepsilon_{\rm HN}$ and $\Delta\varepsilon_{\rm CC}$ are the relaxation strengths, $\tau_{\rm HN}$ and $\tau_{\rm CC}$ the relaxation times, and $\alpha_{\rm HN}$, $\beta_{\rm HN}$ and $\alpha_{\rm CC}$ the spectral width parameters of the HN and CC function, respectively and ω is the circular frequency.

As seen in fig. 3 the BDS spectra of *salol* can be fitted with both the coexisting spectral α and β components up to 238 K. At the next temperature $T = 243$ K, the secondary β peak is completely merged with the α peak and consequently, the spectra can be fitted by considering the structural relaxation only.

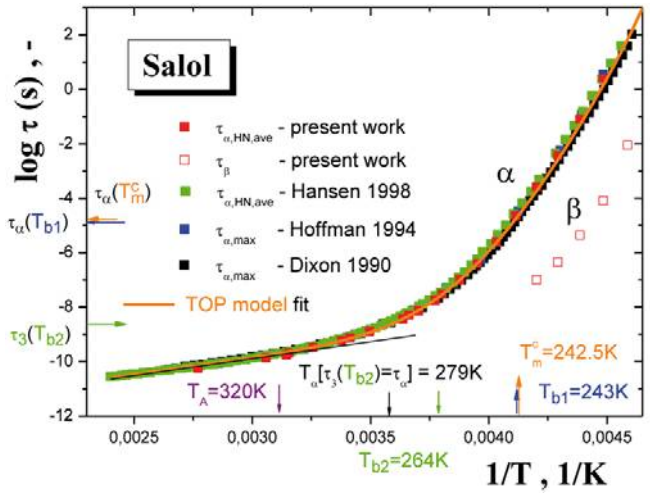

Fig. 4. (Colour on-line) Relaxation times of the α and β process as a function of inverse temperature for *salol* [108,109,122]. The measured data are in very good agreement with those from other authors: Hansen *et al.* [20–22], Dixon *et al.* [94,95] and Hofman *et al.* [96]. The characteristic PALS temperatures T_{b1}^L and T_{b2}^L are depicted by the blue or green arrows, respectively. Test of the M-VFTH expression on all the structural relaxation data for *salol* [20–22,94–96,108,109,122] with the following fitting parameters: $\log \tau_{\alpha,\infty} = -13.5$, $B = 1210.5\,\mathrm{K}$, $\kappa = 0.0589/\mathrm{K}$, $T_m^c = 242.4\,\mathrm{K}$ and $T_0 = 174.5\,\mathrm{K}$.

Figure 4 summarizes the corresponding relaxation times, τ_α and τ_β, in *salol* as obtained from the above-mentioned additive fitting procedure [108,109]. The former are in very good agreement with previous determinations [20–22,94–96]. Further, it is evident that both the α and β relaxation processes exhibit non-Arrhenius character which can be parameterized, *e.g.*, by the corresponding VFTH equation. Thus, the secondary β process can be described satisfactorily by the following VFTH equation: $\tau_\beta(T) = 2\times10^{-12}\exp[1882.1/(T-199)]$. In the case of the primary α process, several phenomenological expressions such as a combination of two VFTH equations [20–22] or the modified M-VFTH equation [45–48] or other formulae [32–41,121,122] can be used to describe the relaxation time data over a sufficiently wide T range. One alternative description of the structural relaxation over a wide T range related to the finding of the limited occurrence of the secondary β relaxation as well as to the T_{b1} effect in the PALS response will be given below.

4 Discussion

4.1 PALS data

The complex course of the PALS response of *salol* in both heating scans No. 1 and 2 characterized by the presence of two discontinuities at around 245 K and 300 K is connected with its phase transformation tendency due to its relatively simple and internally flexible structure. Recent detailed study of the phase transformation behaviour of *salol* by DSC demonstrated the occurrence of the crystallization exoterm on the rapidly cooled sample during the heating DSC run followed by the melting endoterm of the crystallized material [90]. The observed discontinuities in the PALS responses of the transforming *salol* sample are fully consistent with the characteristic DSC temperatures for crystallization being $T_{\mathrm{cr}} \sim 250\,\mathrm{K}$ and for melting of the relatively rapidly cooled material $T_{m1} \sim 305\,\mathrm{K}$, the latter in contrast to $T_{m2} = 317\,\mathrm{K}$ for the very slowly cooled and crystallized sample [90]. The slightly lower characteristic PALS temperatures in comparison with the characteristic DSC ones reflect an essentially longer time scale in accumulation of the PALS data with respect to relatively rapid DSC scanning.

In contrast, the PALS response of *salol* as obtained during cooling of the previously melted at 80 °C sample from RT down to 15 K exhibits the quasi-sigmoidal form of $\tau_3(T)$ dependence which is the typical signature of amorphous glass-forming materials [61–75]. Closer inspection of this PALS response of amorphous *salol* reveals basically four regions of distinct thermal behavior marked as I-IV. First, the low-T region from 15 K up to $\sim 210\,\mathrm{K}$ is followed by a sharply increasing intermediate region between $\sim 215\,\mathrm{K}$ and $\sim 260\,\mathrm{K}$ with two clear sub-regions. Finally, at relatively high temperatures an evolution towards a plateau effect is evident. A phenomenological analysis of these four basic regions in the PALS response of *salol* by a linear fitting [65–69] gives the following linear expressions for the distinct thermal behavior of the o-Ps lifetime with temperature:

For region I from 15 K up to 210 K:

$$\tau_3 = (1.68\pm0.18)\times10^{-3}T+(1.255\pm0.025), \qquad r = 0.935, \tag{2.1}$$

for region II from 215 K up to 240 K:

$$\tau_3 = (1.43\pm0.14)\times10^{-2}T-(1.41\pm0.31), \qquad r = 0.988, \tag{2.2}$$

for region III from 250 K up to 260 K:

$$\tau_3 = (2.56\pm0.03)\times10^{-2}T-(4.145\pm0.865), \qquad r = 0.993, \tag{2.3}$$

and finally, for region IV from 270 K up to 350 K: $\tau_3 = 2.6\,\mathrm{ns}$.

These four distinct thermal regions provide, via the corresponding intersection points, the following three characteristic PALS temperatures depicted as $T_g^{\mathrm{PALS}} = 211\,\mathrm{K}$, $T_{b1}^L = 243\,\mathrm{K}$ and finally, $T_{b2}^L = 264\,\mathrm{K}$.

The first pronounced bend effect in the PALS response at 211 K lies in the vicinity of the thermodynamic glass transition temperature characterizing by similar bend and step effects found in the specific volume measured by dilatometry or in the specific heat measured by DSC, namely at $T_g^{\mathrm{DSC}} = 218\,\mathrm{K}$ [86] or 220 K [85,90]. Thus, it defines the PALS glass transition temperature, T_g^{PALS}. The following rather slight and the final, well-pronounced bend effects arising in the liquid state of *salol* correspond to the relatively characteristic PALS temperatures of $T_{b1}^L/T_g^{\mathrm{PALS}} = 1.15$ or $T_{b2}^L/T_g^{\mathrm{PALS}} = 1.25$, respectively.

Figure 2 displays also the mean free volume, V_h, as a function of temperature. This quantity was obtained by using the standard quantum-mechanical (SQM) model given by semi-empirical Tao-Eldrup-Nakanishi equation relating the observed o-Ps lifetime with the (spherical) free volume hole radius [55–57]

$$\tau_3 = \tau_{3,0}\left\{1 - R_h/(R_h + \Delta R) + (1/2\pi)\sin\left[2\pi R_h/(R_h + \Delta R)\right]\right\}^{-1}, \quad (3)$$

where $\tau_{3,0} = 0.5\,\mathrm{ns}$ is the spin-averaged lifetime of p-Ps and o-Ps and $\Delta R = R_0 - R_h = 1.66\,\text{Å}$ is the thickness of the electron layer about the free-volume hole which was obtained as a parameter from fitting the observed o-Ps lifetimes to known vacancy or free-volume hole sizes in molecular crystals and zeolites [55–57]. In reality, the shape of free-volume entities is not spherical, so that the standard model (eq. (3)) is used in the sense of the mean o-Ps lifetime and subsequently, to estimate the *equivalent* mean hole radius. Then, the corresponding mean hole volume is given by $V_h = (4/3)\pi R_h^3$.

In general, the equivalent hole sizes in the amorphous *salol* from the SQM model are significantly smaller than the van der Waals volume of the *salol* molecule ($V^W_{\mathrm{molecule}} = 186.5\,\text{Å}^3$) over the whole temperature range of our PALS study. This strongly implies that the dynamics of the whole molecule has to be of highly cooperative character. On the other hand, the mean hole size at 240 K is comparable with the vdW volume of phenyl and benzyl groups being $V^W_{\mathrm{group}} = 83.7\,\text{Å}^3$ or $85.2\,\text{Å}^3$, respectively. In the context of the observed course of crystallization above $\sim 240\,\mathrm{K}$ the finding that $V_h > V^W_{\mathrm{group}}$ would suggest that the reorientation of both partial groups of the flexible *salol* molecule could play a certain role during the ordering process in the phase transformation seen in both heating scans in fig. 2.

4.2 The mutual relationships between the PALS and BDS databases for amorphous salol

Returning to the PALS response of amorphous *salol*, its liquid state is characterized by the two PALS temperatures: $T^L_{b1} = 243\,\mathrm{K}$ and $T^L_{b2} = 264\,\mathrm{K}$, corresponding to the relative values $T^L_{b1}/T^{\mathrm{PALS}}_g = 1.15$ or $T^L_{b2}/T^{\mathrm{PALS}}_g = 1.25$, respectively. The first relative value is significantly lower than the typical ranges for the ratio $T^L_{bi}/T^{\mathrm{PALS}}_g$ found so far for most other small molecular and polymeric glass formers studied, being $T^L_{b1}/T^{\mathrm{PALS}}_g = 1.2$–$1.4$ [65–69]. On the other hand, the other one lies at the lower value limit of $T^L_{b2}/T^{\mathrm{PALS}}_g = 1.2$–$1.7$ [65–72] being close to these ratios for *propylene carbonate* (*PC*) [72,73], *phenolphthalain-dimethyl-ether (PDE)* [74] and *poly(methyl phenylsiloxane)* [75]. Note that the latter relative PALS temperature compares well with the ratio $T^L_{k\tau 3}/T^{\mathrm{PALS}}_g = 1.23$ by Dlubek *et al.* from summarizing paper on a series of small molecule glass formers [74], though the original paper on *salol* indicates a ratio of 1.36 due to melting of the *crystallized* material formed during the heating regime of their PALS measurement [100].

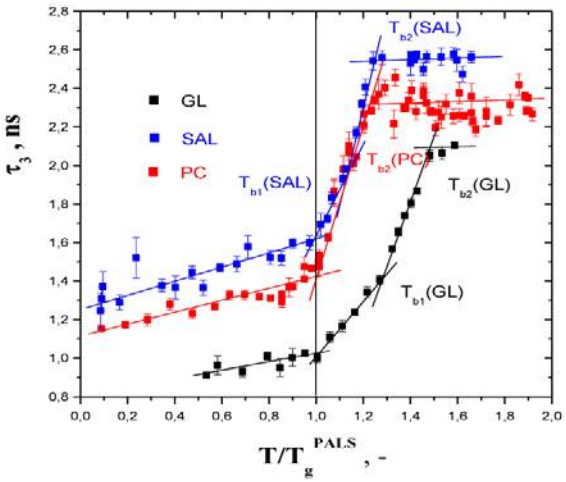

Fig. 5. PALS response of *salol* in comparison with those for *glycerol* [66] and *propylene carbonate* [73] in the normalized T coordinate. For the mutual relationship between the chemical composition, the corresponding type of intermolecular interactions and the characteristic PALS temperatures, see the text.

It is of interest to compare the τ_3 *vs.* T plot and the corresponding PALS temperatures for *salol* which has an intermediate degree of H-bonding as well as an intermediate fragility with some selected small molecule glass formers with different type and extent of intermolecular interactions and different fragilities. Figure 5 compares the PALS response of *salol* with those for *glycerol* (GL) [66] and PC [73] as the typical representatives of strong and fragile substances with intermolecular H-bond or vdW interaction forces, respectively. The o-Ps lifetimes for *salol* lie very significantly above those for GL due to weaker association and less tighter molecular packing. They also exceed those for PC in both the glassy and normal liquid states, having smaller vdW volume of $86\,\text{Å}^3$ compared to $186.5\,\text{Å}^3$ for *salol*. The latter finding would indicate that the difference in the free volume, arising from the frozen static disorder in the glassy state and the dynamic disorder in the normal liquid, is connected with the internal flexibility and H-bonding tendency of *salol* in contrast to the rigid and compact molecule of PC. In addition, the lower $T^L_{b1}/T^{\mathrm{PALS}}_g$ for *salol* in comparison to GL may be also ascribed to the smaller extent of H-bonding, while PC exhibits a weak T^L_{b1} effect only [73]. The ratio $T^L_{b2}/T^{\mathrm{PALS}}_g$ for the plateau effect for the intermediate *salol* lies consistently and significantly below that for the strong GL glass former and is rather close to that for very fragile PC. All these findings seem to suggest that not only the type of intermolecular interactions among the molecules determines the absolute τ_3 values and the related free-volume microstructure of the respective matrices, but also other factor(s) is (are) of relevance.

In our effort to find the causes of these significantly lower relative PALS temperatures for *salol*, it is useful to search for potential relationships to the dynamic heterogeneity as expressed by the characteristic dynamic temperatures from phenomenological and theoretical studies.

Thus, concerning the former aspect, the derivative analysis of the structural relaxation time as a function of temperature over a wide T range revealed the existence of two different dynamic regions with the characteristic Stickel temperature, $T_B^{\rm ST} = 265\,{\rm K}$ [20–22]. This is in very good agreement with the T_{b2}^L value. This indicates that the occurrence of the plateau effect in the PALS response is closely connected with a qualitative change in the structural relaxation. Recently, Roland *et al.* reported a bit lower values for $T_B^{\rm ST}$ of *salol* being 253 K [27–31] and 254 K [35] based on the same derivative analysis of their own dielectric data or the viscosity data [91–93], respectively. The small difference between their $T_B^{\rm ST}$ values with respect to the original Stickel value is due to the different definition used at the data evaluation [29], whereby the original definition based on the upper-T deviation from linearity of the Stickel operator is more consistent with the PALS response. Similar T_{b2}^L *vs.* $T_B^{\rm ST}$ correlations occur also in GL and PC [66,72,73].

Next, in the context with the plateau effect it is of interest to verify an accompanying aspect of the T_{b2}^L rule $\tau_\alpha(T_{b2}^L) \sim 10^{-9}\,{\rm s}$, *i.e.*, the $\tau_3(T_{b2}^L) = \tau_\alpha(T_{b2}^L)$ relation between the PALS and BDS time scales observed often for many small molecular and polymer systems [65,78]. From fig. 4 it becomes evident that this relation is not fulfilled because the α identity temperature $T_\alpha[\tau_3(T_{b2}^L) = \tau_\alpha] \cong 280\,{\rm K}$ is significantly —about 15 K— higher than T_{b2}^L. Thus, despite the $T_{b2}^L \cong T_B^{\rm ST}$ correlation, the T_{b2}^L rule is not valid for *salol*. A similar finding was very recently observed for another small molecular glass former of vdW type PDE of close fragility ($m_g = 78$ [11]) and because of the internal flexibility of PDE it was tentatively attributed to the intra-molecular degrees of freedom via ring flipping in the PDE molecule [123]. Since *salol* consists of highly flexible molecules with relatively small phenyl and benzyl groups, the hypothesis of "smearing" of free volume via the faster mobility of these groups of the *salol* molecule resulting into a plateau effect in the PALS response might be of relevance too. Note that for *glycerol* and *propylene carbonate* with the intrinsically rigid molecules both the $T_{b2}^L = T_B^{\rm ST}$ correlation as well as the $\tau_3(T_{b2}^L) = \tau_\alpha(T_{b2}^L)$ relationship have been found to be valid [66,73] in apparent consistency with the hypothesis of internal mobility.

Finally, we discuss the T_{b1}^L effect in *salol* at $1.15T_g$. From the decomposed BDS spectra it follows that the EW caused by the secondary process can be observed up to 238 K, *i.e.*, when increasing the temperature it becomes completely merged with the process close below T_{b1}^L. On the other hand, the T_{b1}^L rule [65,78] appears to be valid for *salol* because $\tau_\alpha(T_{b1}^L) = 2.2 \times 10^{-5}\,{\rm s}$ suggesting that some aspect of the primary α process plays a role in the slight bend effect at T_{b1}^L. Indeed, a direct inspection of the BDS spectra of *salol* (fig. 3) confirms that at the equivalent frequency of the o-Ps lifetime (about 100 MHz) the dielectric loss starts to be governed by the high-f tail of the α peak just at around $T = 243\,{\rm K}$ being close to T_{b1}^L. In contrast, at lower temperatures the EW represents the main contribution to the loss at 100 MHz. Then, we conclude that the slight bend effect at T_{b1}^L is related to the onset of the influence of the primary α process on the PALS response of *salol* when temperature is increasing.

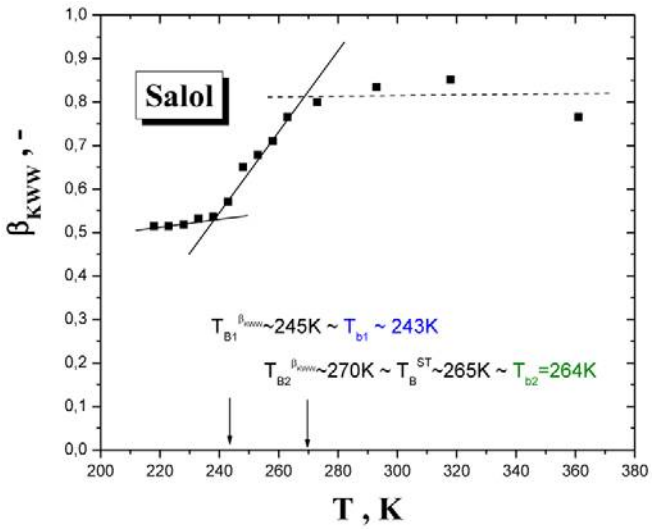

Fig. 6. Non-exponentiality parameter, $\beta_{\rm KWW}$, as a function of temperature for *salol*. Three distinct regions characterized by the characteristic temperatures $T_{B1}^{\beta_{\rm KWW}}$ and $T_{B2}^{\beta_{\rm KWW}}$ correlating with the characteristic PALS temperatures T_{b1}^L or T_{b2}^L, respectively, are evident.

In the previous paragraphs, the PALS response has been discussed in relation to the dynamic heterogeneity expressed by the qualitative changes in the *mean* relaxation time parameters of the primary process at $T_B^{\rm ST}$ and its onset as well as the diminishing of the secondary processes connected with T_{b2}^L or T_{b1}^L, respectively. In addition, further connections between both the characteristic PALS temperatures and the changes in the spectral parameters, namely, the spectral width of the main peak characterizing the structural relaxation times distribution can be found. The structural relaxation time distribution is usually quantified by the non-exponentiality parameter, $\beta_{\rm KWW}$, from the Kohlrausch-Williams-Watts (KWW) equation. Thus, fig. 6 shows the temperature dependence of the $\beta_{\rm KWW}$ parameter calculated from the spectral quantities $\alpha_{\rm HN}$ and $\beta_{\rm HN}$ as obtained from the fitted HN function via the conversion formula: $(1-\alpha_{\rm HN})\beta_{\rm HN} = \beta_{\rm KWW}^{1.23}$ [124]. The converted $\beta_{\rm KWW}$ *vs.* T dependence is consistent with previous reports from dielectric relaxation [37] and from light scattering [97,98,125]. The straight lines in fig. 6 suggest three regions of distinct behavior of the non-exponentiality parameter, which presumably is inversely related to the extent of the dynamic heterogeneity above T_g [126]. Similar changes of $\beta_{\rm KWW}$ in various materials were reported in ref. [127] and the influence of the fragility was pointed out. They correlate with the corresponding three regions in the PALS response (fig. 2) with similar characteristic dynamic and PALS temperatures: $T_{B1}^{\beta_{\rm KWW}} \cong T_{b1}^L$ and $T_{B2}^{\beta_{\rm KWW}} \cong T_{b2}^L$. These correlations appear to be further manifestations of the dynamic character of both crossover effects in the PALS response in the liquid state of *salol*. Note that usually two more or less distinct regions in

β_{KWW} *vs.* T plots are observed for the majority of small molecules [24,73,84,126] as well as polymeric glass formers [25,26]. The rather rare presence of two pronounced bend effects in the β_{KWW} *vs.* T plot of the intermediate fragile *salol* in contrast to the rigid strong GL and the very fragile PC, especially that at the lower temperature, may be a reflection of the influence of internal flexibility on the structural relaxation of *salol*. However, more findings concerning the mutual relationships between the PALS response and the structural relaxation distribution are needed to be accumulated.

4.3 Structural relaxation in terms of the TOP model and its connections with the PALS response and secondary dynamics

As mentioned in the BDS part, the structural relaxation time as a function of temperature of *salol* over a sufficiently wide temperature range can be described in several ways. One group of phenomenological expressions is represented by the VFTH equation and its combinations [20–22] or by the recent modified M-VFTH equation [45–48]. Another one consists of very recent expressions with [32–41] or without any divergence or characteristic temperatures such as those based on the models by Avramov [121,128] or Mauro *et al.* [129]. A recent treatment of the present relaxation times can be found in [122]. Here, we focus on a test of the modified VFTH equation because of the potential of this model to give some simultaneous insight into the PALS and BDS findings [73,81, 84]. Figure 4 shows also a fit with the M-VFTH formula given by

$$\tau_\alpha(T) = \tau_{\alpha\infty} \exp[E^*_\tau/RT] \exp[BF(T)/(T - T_0)], \quad (4.1)$$

where $\tau(T)$ is the structural relaxation time, τ_∞ is the pre-exponent factor, E^*_τ is the activation energy above $T^*_m \approx T_A$, T_0 is the divergence temperature, B is the coefficient and $F(T)$ is a probability function for *solid*-like domains. The latter quantity is defined as

$$F(T) = 1/\{\exp[\kappa(T - T^c_m)] + 1\}, \quad (4.2)$$

where κ describes the sharpness of the probability function between *solid*-like and *liquid*-like domains and T^c_m is the characteristic TOP temperature. This is the critical temperature where the free energy of a crystallizing liquid is equal to that of the crystal $\Delta G_{\mathrm{lq}} = \Delta G_{\mathrm{cr}}$ or, in the general case of non-crystallizing glass-formers, the free energy of a non-crystallizing liquid is equal to that of a solid: $\Delta G_{\mathrm{lq}} = \Delta G_{\mathrm{sol}}$. This expression describes well our BDS data on *salol* [122] over the temperature range from 212 K up to 361 K of our BDS measurements. Similar results with slightly modified parameters were obtained from fitting the data restricted up to 320 K [29] in the original work by Tanaka [48] as well as from fitting the compilation of all the published structural relaxation times [20–22, 94–96,108,109,122] presented in fig. 4 over an essentially wider T range up to 420 K. This indicates the robustness of the M-VFTH expression to account for the structural relaxation time data of *salol*.

Moreover, the author of the TOP model was able to describe also the temperature evolution of the sub-peak of the structure factor $S(q)$ of *salol* from a detailed X-diffraction study [42], which is a measure of the medium-range order by means of the two parameters κ and T^c_m of the probability function $F(T)$ resulting from fitting the structural relaxation data by eq. (4.1). This finding is interpreted as an argument in favor of the *solid*-like and *liquid*-like picture behind the TOP model [48]. A very recent structural study of *salol* by means of Fourier-transform infrared spectroscopy [89] confirmed the cluster-like heterogeneous character of supercooled liquid below ~ 270 K and the formation of the ordered clusters at around 250 K. It is of interest that both these temperatures are close to $T^{\mathrm{ST}}_B \sim T^{\beta_{\mathrm{KWW}}}_{B2}$ correlating with T^L_{b2} or to $T^{\beta_{\mathrm{KWW}}}_{B1}$ correlating with T^L_{b1}, respectively.

The characteristic TOP temperature of *salol* from the M-VFTH equation of the TOP model, T^c_m, is in good agreement with that of the T^L_{b1} effect in the PALS response in fig. 2 as well as with the BDS findings in figs. 3, 4 and 6. Thus, within the framework of this model, the change of the slope in the τ_3 *vs.* T plot is situated at around 240 K where the *liquid*-like domains start to dominate over the *solid*-like ones in full consistency with the change in the complete merging of the secondary excess wing relaxation with the structural relaxation peak in the BDS spectra in fig. 3. The mean structural relaxation time at the characteristic TOP temperature, $\tau_\alpha(T^c_m)$, is consistent with the T^L_{b1} rule. As for the dielectric relaxation data, within the TOP model, the occurrence of the secondary relaxation seems to be associated with the dominating *solid*-like domains in the deeply supercooled *salol*. And finally, the two crossovers in the dynamic heterogeneity expressed by the non-exponentiality parameter of the structural relaxation seem to be connected with a change in the dominance of the *liquid*-like domains over the *solid*-like ones and to the overwhelming dominance of the *liquid*-like regions probably modulated by the internal mobility of the flexible *salol* molecules.

5 Summary and conclusion

A detailed study of glass-forming *salol* has been provided combining PALS, performed in a very broad temperature interval, and BDS, covering an exceptionally broad frequency range. A detailed phenomenological analysis of the annihilation and dynamic databases has been carried out. Several well-known and some new correlations between the PALS and BDS data sets have been confirmed or revealed.

In particular, the $T^L_{b2} \cong T^{\mathrm{ST}}_B$ correlation is valid implying that the dramatic change in the PALS response is related to the qualitative change in the character of the primary α process at the T^{ST}_B. However, the $\tau_3(T^L_{b2}) = \tau_\alpha(T^L_{b2})$ relationship is not valid, *i.e.*, the plateau effect at T^L_{b2} in the PALS response is not correlated with the primary α process and probably, some faster internal degree

of freedom due to internal flexibility of the *salol* molecule is included. The T_{b1}^L rule in the PALS response is still valid. The bend effect at T_{b1}^L is related to some aspect of the structural relaxation, *i.e.*, the onset of the dominance of the α process instead of the excess wing at the frequency corresponding to the o-Ps lifetime. Moreover, both the slight bend at T_{b1}^L and the pronounced plateau at T_{b2}^L in the PALS response of amorphous *salol* correlate very closely with two crossovers in the spectral shape parameter of the structural relaxation at $T_{B1}^{\beta\mathrm{KWW}}$ or $T_{B2}^{\beta\mathrm{KWW}}$, respectively. Finally, the structural relaxation over a wide T range can be described by means of the modified VFTH equation with the characteristic TOP parameter, T_{rp}^c, being close to the characteristic PALS temperature T_{b1}^L.

In summary, numerous correlations of the PALS response of *salol* with the spectral and relaxation parameters of its primary and secondary relaxation dynamics as seen by BDS have been established. Within the framework of the TOP model, these findings suggest the possible validity of the *solid*-like and *liquid*-like domain picture for the disordered *salol* sample.

The authors J.B. and O.Š. would like to thank the VEGA Agency, Slovakia for support of this research by the grants No. 2/0014/09 or 2/0099/10, respectively.

References

1. M.D. Ediger, C.A. Angell, S.R. Nagel, J. Phys. Chem. B **100**, 13200 (1996).
2. C.A. Angell, K.L. Ngai, G.B. McKenna, P.F. McMillan, S.W. Martin, J. Appl. Phys. **88**, 3113 (2000).
3. P.G. DeBenedetti, F.H. Stillinger, Nature **410**, 259 (2001).
4. For review: a series of special issues from *International Discussion Meeting on Relaxations in Complex Systems* in J. Non-Cryst. Solids **131-133** (1991); *ibid.* **172-174** (1994); *ibid.* **235-237** (1998); *ibid.* **307-310** (2002); **352** (2006) and **357** (2010).
5. D.C. Champeney, R.B.N. Joarder, J.C. Dore, Mol. Phys. **58**, 337 (1986).
6. R.L. Leheny, N. Menon, S.R. Nagel, D.L. Price, K. Suzuya, P. Thiyagarajan, J. Chem. Phys. **105**, 7783 (1996).
7. B. Frick, D. Richter, C. Ritter, Europhys. Lett. **9**, 557 (1989).
8. E.W. Fischer, Physica A **201**, 183 (1993).
9. A.P. Sokolov, Endeavour **21**, 109 (1997).
10. K.L. Ngai, J. Non-Cryst. Solids **275**, 7 (2000).
11. M. Beiner *et al.*, J. Non-Cryst. Solids **279**, 126 (2001).
12. R. Böhmer, Curr. Opin. Solid State Mater. Sci. **3**, 378 (1998).
13. H. Silescu, J. Non-Cryst. Solids **243**, 81 (1999).
14. M.D. Ediger, Annu. Rev. Phys. Chem. **51**, 99 (2000).
15. R. Richert, J. Phys.: Condens. Matter **14**, R703 (2002).
16. A.J. Barlow, J. Lamb, A.J. Matheson, Proc. R. Soc. London, Ser. A **292**, 322 (1966).
17. D.J. Plazek, J.H. Magill, J. Chem. Phys. **45**, 3038 (1966).
18. K.L. Ngai, J.H. Magill, D.J. Plazek, J. Chem. Phys. **112**, 1887 (2000).
19. A. Schönhals, F. Kremer, A. Hofmann, E.W. Fischer, E. Schlosser, Phys. Rev. Lett. **70**, 3459 (1993).
20. F. Stickel, E.W. Fischer, R. Richert, J. Chem. Phys. **102**, 6251 (1995).
21. F. Stickel, E.W. Fischer, R. Richert, J. Chem. Phys. **104**, 2043 (1996).
22. C. Hansen, F. Stickel, R. Richert, E.W. Fischer, J. Chem. Phys. **108**, 6408 (1998).
23. A. Schönhals, Europhys. Lett. **56**, 815 (2001).
24. C. Leon, K.L. Ngai, J. Phys. Chem. B **103**, 4045 (1999).
25. K.L. Ngai, C.M. Roland, Polymer **43**, 567 (2002).
26. A. Alegria, J. Colmenero, P.O. Mari, I.A. Campbell, Phys. Rev. E **59**, 6888 (1999).
27. R. Casalini, M. Paluch, C.M. Roland, J. Chem. Phys. **118**, 5701 (2003).
28. R. Casalini, M. Roland, Phys. Rev. Lett. **92**, 245702 (2004).
29. R. Casalini, C.M. Roland, Phys. Rev. B **71**, 014210 (2005).
30. C.M. Roland, R. Casalini, J. Non-Cryst. Solids **351**, 2581 (2005).
31. M. Roland, Soft Matter **4**, 2314 (2008).
32. M.H. Cohen, G.S. Grest, Phys. Rev. B **20**, 1077 (1979).
33. G.S. Grest, M.H. Cohen, Phys. Rev. B **28**, 4113 (1980).
34. M.H. Cohen, G. Grest, Adv. Chem. Phys. **48**, 455 (1981).
35. M. Paluch, R. Casalini, C.M. Roland, Phys. Rev. E **67**, 021508 (2003).
36. K.L. Ngai, Comm. Solid State Phys. **9**, 141 (1979).
37. K.L. Ngai, J. Non-Cryst. Solids **9**, 1107 (2003).
38. R. Casalini, K.L. Ngai, C.M. Roland, Phys. Rev. E **68**, 014201 (2003).
39. D. Kivelson, S.A. Kivelson, X.L. Zhao, Z. Nussinov, G. Tarjus, Physica A **219**, 27 (1995).
40. D. Kivelson, G. Tarjus, X.L. Zhao, S.A. Kivelson, Phys. Rev. E **53**, 751 (1996).
41. D. Kivelson, G. Tarjus, J. Non-Cryst. Solids **235-237**, 86 (1998).
42. E. Eckstein, J. Qian, R. Hentschke, T. Thurn-Albert, W. Steffen, E.W. Fischer, J. Chem. Phys. **113**, 4751 (2000).
43. E. Fischer, A. Sakai, in *Heterophase Fluctuations in Supercooled Liquids and Polymers*, *AIP Conf. Proc.* No. 469, edited by M. Tokuyama, I. Oppenheim (1999) p. 325.
44. E.W. Fischer, A. Bakai, A. Patkowski, W. Steffen, L. Reinhardt, J. Non-Cryst. Solids **307–310**, 584 (2002).
45. H. Tanaka, J. Phys.: Condens. Matter **10**, L207 (1998).
46. H. Tanaka, J. Phys.: Condens. Matter **11**, L159 (1999).
47. H. Tanaka, J. Chem. Phys. **111**, 3163 (1999); and 3175.
48. H. Tanaka, J. Non-Cryst. Solids **351**, 3371 (2005); 3385 and 3396.
49. A. Bondi, *Physical Properties of Crystals, Liquids and Glasses* (Wiley, New York, 1968).
50. J.D. Ferry, *Viscoelastic Properties of Polymers*, 3rd ed. (Wiley, New York, 1980).
51. J. Crank, G. Park (Editors), *Diffusion in Polymers* (Academic Press, New York, 1968).
52. G. Dlubek, in: *Encyclopedia of Polymer Science and Technology* (Wiley & Sons, 2008).
53. Y.C. Jean, P.E. Malton, D.M. Schraeder (Editors), *Principles and Application of Positron and Positronium Chemistry* (World Scientific, Singapore, 2003).
54. J. Bartoš, in: *Encyclopedia of Analytical Chemistry*, edited by R.A. Meyers (Wiley & Sons, Chichester, 2000) p. 7968.

55. S. Tao, J. Chem. Phys. **56**, 5499 (1972).
56. M. Eldrup, D. Ligthbody, J.N. Sherwood, Chem. Phys. **63**, 51 (1981).
57. H. Nakanishi, Y.C. Jean, S.J. Wang, in *Positron Annihilation Studies of Fluids*, edited by S.C. Sharma (World Scientific, Singapore, 1988), p. 292.
58. H.S. Landes, S. Berko, A.J. Zuchelli, Phys. Rev. **103**, 828 (1956).
59. W. Brandt, S. Berko, W.W. Walker, Phys. Rev. **120**, 1289 (1960).
60. E.L.E. Kluth, H. Clarke, B.G. Hogg, J. Chem. Phys. **40**, 3180 (1964).
61. W. Brandt, I. Spirn, Phys. Rev. **142**, 231 (1966).
62. R.A. Pethrick, F.M. Jacobsen, O.E. Mogensen M. Eldrup, J. Chem. Soc. Faraday Trans. II **78**, 287 (1982).
63. Y.C. Jean, T.C. Sandreczki, D.P. Ames, J. Polym. Sci. B, Polym. Phys. **24**, 1247 (1986).
64. J. Krištiak, O. Šauša, P. Bandžuch, .J. Bartoš, J. Rad. Nucl. Chem. **210**, 563 (1996).
65. J. Bartoš, O. Šauša, P. Bandžuch, J. Zrubcová, J. Krištiak, J. Non-Cryst. Solids **307–310**, 417 (2002).
66. J. Bartoš, O. Šauša, J. Krištiak, T. Blochowicz, E. Rössler, J. Phys.: Condens. Matter **13**, 11 473 (2001).
67. D. Kilburn, J. Wawryszczuk, G. Dlubek, J. Pionteck, R. Hässler, M.A. Alam, Macromol. Chem. Phys. **207**, 721 (2006).
68. J. Wu, G. Huang, Q. Pan, L. Qu, Y. Zhu, B. Wang, Appl. Phys. Lett. **89**, 121904 (2006).
69. W. Salgueiro, A. Somoza, G. Consolati, F. Quasso, A. Marzocca, Phys. Status Solidi C4 **10**, 3771 (2007).
70. R.A. Pethrick, F.M. Jacobsen, O.E. Mogensen, M. Eldrup, J. Chem. Soc. Faraday Trans. II **76**, 225 (1980).
71. J.R. Stevens, S.H. Chung, P. Horoyski, K.R. Jeffrey, J. Non-Cryst. Solids **172-174**, 1207 (1994).
72. K.L. Ngai, L.R. Bao, A.F. Yee, C.L. Soles, Phys. Rev. Lett. **87**, 215901 (2001).
73. J. Bartoš, V. Majernik, M. Iskrová, O. Šauša, J. Krištiak, P. Lunkenheimer, A. Loidl, J. Non-Cryst. Solids **356**, 794 (2010).
74. G. Dlubek, M.Q. Shaik, K. Raetzke, M. Paluch, F. Faupel, J. Phys.: Condens. Matter **22**, 235104 (2010).
75. G. Dlubek, M.Q. Shaik, R. Krause-Rehberg, M. Paluch, J. Chem. Phys. **126**, 024906 (2007).
76. P. Lunkenheimer, U. Schneider, R. Brand, A. Loidl, Contemp. Phys. **41**, 15 (2000).
77. F. Kremer, A. Schönhals (Editors), *Broadband Dielectric Spectroscopy* (Springer, Berlin, 2002).
78. J. Bartoš, D. Račko, O. Šauša, J. Krištiak, *Soft Matter under Exogenic Impacts. Fundamentals and Emerging Technologies*, ARW NATO Ser., edited by S.J. Rzoska, V. Mazur (Springer-Verlag, Berlin, 2007) p. 113.
79. J.T. Bendler, J.J. Fontanella, M. Shlesinger, J. Bartoš, O. Šauša, J. Krištiak, Phys. Rev. E **71**, 031508 (2005).
80. J. Bartoš, A. Alegría, O. Šauša, M. Tyagi, D. Gómez, J. Krištiak, J. Colmenero, Phys. Rev. E **76**, 031503 (2007).
81. J. Bartoš, G. Schwartz, O. Šauša, A. Alegría, J. Krištiak, J. Colmenero, J. Non-Cryst. Solids **356**, 782 (2010).
82. S. Pawlus, J. Bartoš, O. Šauša, J. Krištiak, M. Paluch, J. Chem. Phys. **124**, 104505 (2006).
83. J. Bartoš, O. Šauša, D. Račko, J. Krištiak, J.J. Fontanella, J. Non-Cryst. Solids **351**, 2599 (2005).
84. J. Bartoš, O. Šauša, M. Köhler, H. Švajdlenková, P. Lunkenheimer, J. Krištiak, A. Loidl, J. Non-Cryst. Solids **357**, 376 (2011).
85. R. Richert, C.A. Angell, J. Chem. Phys. **108**, 9016 (1998).
86. R. Böhmer, K.L. Ngai, C.A. Angell, D.J. Plazek, J. Chem. Phys. **99**, 4201 (1993).
87. J.H. Bilgram,U. During, M. Wachter, P. Seiler, J. Crystal Growth **57**, 1 (1982).
88. R.B. Hammond, M.J. Jones, K.J. Roberts, H. Kutzke, H. Klapper, Z. Kristallogr. **217**, 484 (2002).
89. J. Baran, N.A. Davidova, Phys. Rev. E **81**, 031503 (2010).
90. J.J. Moura Ramos, N.T. Correiaa, H.P. Diogob, Phys. Chem. Chem. Phys. **6**, 793 (2004).
91. W.T. Laughlin, D.R. Uhlmann, J. Phys. Chem. **76**, 2317 (1072).
92. M. Cukierman, J.W. Lane, D.R. Uhlmann, J. Chem. Phys. **59**, 3639 (1973).
93. G.D. Enright, B.P. Stoicheff, J. Chem. Phys. **64**, 3658 (1976).
94. P.K. Dixon, Phys. Rev. E **42**, 8179 (1990).
95. P.K. Dixon, L. Wu, S.R. Nagel, B.D. Williams, J.P. Carini, Phys. Rev. Lett. **65**, 1108 (1990).
96. A. Hofmann, F. Kremer, E.W. Fischer, A. Schönhals, in *Disorder Effects on Relaxational Processes*, edited by R. Richert, A. Blumen (Springer, Berlin, 1994) p. 309.
97. G. Li, W.M. Du, A. Sakai, H.Z. Cummins, Phys. Rev. A **46**, 3343 (1992).
98. C. Dreyfus, M.J. Lebon, H.Z. Cummins, J. Toulouse, B. Bonello, R.M. Pick, Phys. Rev. Lett. **69**, 366 (1992).
99. L. Andreozzi, M. Bannoli, M. Faeti, M. Giordano, J. Non-Cryst. Solids **303**, 262 (2002).
100. G. Dlubek, M.Q. Shaikh, K. Raetzke, F. Faupel, J. Pionteck, M. Paluch, J. Chem. Phys. **130**, 144906 (2009).
101. J. Krištiak, J. Bartoš, K. Krištiaková, P. Bandžuch, Phys. Rev. B **49**, 6601 (1994).
102. P. Kirkegaard, M. Eldrup, O.E. Mogensen, N.J. Pedersen, Comput. Phys. Commun. **23**, 307 (1989).
103. U. Schneider, P. Lunkenheimer, A. Pimenov, R. Brand, A. Loidl, Ferroelectrics **249**, 89 (2001).
104. U. Schneider, P. Lunkenheimer, R. Brand, A. Loidl, Phys. Rev. E **59**, 6924 (1999).
105. R. Böhmer, M. Maglione, P. Lunkenheimer, A. Loidl, J. Appl. Phys. **65**, 901 (1989).
106. A.A. Volkov, Yu.G. Goncharov, G.V. Kozlov, S.P. Lebedev, A.M. Prokhorov, Infrared Phys. **25**, 369 (1985).
107. A.A. Volkov, G.V. Kozlov, S.P. Lebedev, A.M. Prokhorov, Infrared Phys. **29**, 747 (1989).
108. R. Wehn, *Dielektrische Spektroskopie zur Untersuchung der Glasdynamik im Nichtgleichgewicht* (Cuivillier, Göttingen, 2010).
109. M. Köhler, *Relaxation, Rattling and Decoupling* (Mensch und Buch, Berlin, 2010).
110. A. Kudlik, S. Benkhof, T. Blochowicz, T. Tschirwitz, E. Rössler, J. Mol. Struct. **479**, 201 (1999).
111. U. Schneider, R. Brand, P. Lunkenheimer, A. Loidl, Phys. Rev. Lett. **84**, 5560 (2000).
112. P. Lunkenheimer, R. Wehn, Th. Riegger, A. Loidl, J. Non-Cryst. Solids **307-310**, 336 (2002).
113. A. Döß, M. Paluch, H. Sillescu, G. Hinze, Phys. Rev. Lett. **88**, 095701 (2002).
114. R. Casalini, M. Paluch, C.M. Roland, J. Phys. Chem. A **107**, 2369 (2003).
115. P. Lunkenheimer, A. Pimenov, M. Dressel, Yu.G. Goncharov, R. Böhmer, A. Loidl, Phys. Rev. Lett. **77**, 318 (1996).

116. P. Lunkenheimer, A. Pimenov, A. Loidl, Phys. Rev. Lett. **78**, 2995 (1997).
117. M. Köhler, P. Lunkenheimer, Y. Goncharov, R. Wehn, A. Loidl, J. Non-Cryst. Solids **356**, 529 (2010).
118. S. Kastner, M. Köhler, Y. Goncharov, P. Lunkenheimer, A. Loidl, J. Non-Cryst. Solids **357**, 510 (2011).
119. S. Havriliak, S.N. Negami, J. Polym. Sci. C **14**, 99 (1966).
120. K.S. Cole, R.H. Cole, J. Chem. Phys. **9**, 341 (1941).
121. R. Casalini, U. Mohanty, C.M. Roland, J. Chem. Phys. **125**, 014505 (2006).
122. P. Lunkenheimer, S. Kastner, M. Köhler, A. Loidl, Phys. Rev. E **81**, 051504 (2010).
123. G. Dlubek, M.Q. Shaikh, K. Raetzke, F. Faupel, M. Paluch, Phys. Rev. E **78**, 051505 (2008).
124. F. Alvarez, A. Alegria, J. Colmenero, Phys. Rev. B **44**, 7306 (1991).
125. S. Bhattacharyya, B. Bagchi, P. Wolynes, Proc. Natl. Acad. Sci. U.S.A. **105**, 16077 (2008).
126. K. Trachenko, C.M. Roland, R. Casalini, J. Phys. Chem. B **112**, 5111 (2008).
127. L.M. Wang, R. Richert, Phys. Rev. B **76**, 064201 (2007).
128. I. Avramov, J. Chem. Phys. **95**, 4439 (1991).
129. J.C. Mauro, Y. Yue, A.J. Ellison, P.K. Gupta, D.C. Allan, Proc. Natl. Acad. Sci. U.S.A. **106**, 19780 (2009).